Robotica (2008) volume 26, pp. 143–156. © 2007 Cambridge University Press
doi:10.1017/S0263574707003670 Printed in the United Kingdom

Full formation control for autonomous helicopter groups

Farbod Fahimi

Department of Mechanical Engineering, University of Alberta, Edmonton, AB T6G 2G8, Canada

(Received in Final Form: June 10, 2007. First published online: August 22, 2007)

SUMMARY

This paper reports the design of sliding-mode control laws for controlling multiple small-sized autonomous helicopters in arbitrary formations. Two control schemes, which are required for defining arbitrary three-dimensional formation meshes, are discussed. In the presented leader–follower formation control schemes, each helicopter only needs to receive motion information from at most two neighboring helicopters. A nonlinear six-degree-of-freedom dynamic model has been used for each helicopter. Four control inputs, the main and the tail rotor thrusts, and the roll and pitch moments, are assumed. Parameter uncertainty in the dynamic model and wind disturbance are considered in designing the controllers. The effectiveness and robustness of these control laws in the presence of parameter uncertainty in the dynamic model and wind disturbances are demonstrated by computer simulations.

KEYWORDS: Formation control, Autonomous aerial vehicle, Unmanned helicopter, Leader–follower, Sliding mode control.

1. Introduction

Coordinating the behavior of multiple robots, aircrafts, spacecrafts, underwater vessels, and surface vehicles has been studied by many researchers. Application of coordinating the behavior of these vehicles is different, however, the fundamental approaches are similar. In all of these applications, the goal is to coordinate multiple agents to accomplish an objective. The approaches used by researchers to achieve this goal can be roughly categorized under either leader–follower, behavior-based, or virtual structure approaches.

The basic idea of the leader–follower approaches is that a vehicle is designated to track the position and orientation of another vehicle with some prescribed offset, which can be time varying. Numerous variations of this theme exist, including forming a chain (vehicle i follows vehicle $i-1$), defining multiple leaders, and tree topologies. The positive point of the leader–follower approaches is that specifying a single quantity, the leader's motion, directs the group behavior. The weakness, however, is that the leader is a single point of failure for the formation. Also, there is no explicit feedback to the formation. Therefore, the leader cannot be informed if it is moving too fast for the follower vehicles to track.

* Corresponding author. E-mail: ffahimi@ualberta.ca

The mobile robotics community have utilized the leader–follower approach for different purposes, to control a group of robots to move a box,[1] to control the change of formation for multiple robots in environments with obstacles via feedback linearization,[2] to capture/enclose a target by mobile robots via forming troop formationsm,[3] and to investigate the platoon problem in intelligent highways.[4] Both holonomic and nonholonomic kinematic models have been used for controller design. There have been a number of leader–follower studies by spacecraft researchers. In ref. [5], different leader–follower techniques are discussed. Based on this approach, several control laws are derived that keep the formation and the relative attitude of a spacecraft with respect to its nearest neighbor. In other researches, actuator saturation[6] and common space disturbances[7] are considered in designing leader–follower formation controllers. In ref. [8], the leader–follower approach to satellite formation keeping in earth orbit is described.

In behavior-based approaches, several desired behaviors are prescribed for each agent including formation keeping, goal seeking, and obstacle avoidance. The control action of each agent is a weighted average of the control for each behavior. Behavior-based approaches lend themselves to a decentralized implementation and deal with multiple competing objectives very well. However, most of these approaches cannot explicitly define the group behavior. Because of the lack of an explicit definition of the group behavior, it is difficult to guarantee some characteristics of the formation (e.g., stability). For some nonstochastic behavior-based approaches in which the behaviors are defined based on virtual forces that are motivated by natural physics laws, behavioral constraints can be proved.[9]

A behavior-based approach to formation control for mobile robots is derived based on averaging competing behaviors including collision avoidance, formation keeping, and goal seeking.[12] Unpredicted behaviors may occur due to the fact that the competing behaviors are averaged. Creating line and circle formations by mobile robots is investigated using behavior-based approaches.[11] The different behaviors are usually defined by potential field functions. Some researchers have used the potential field method exclusively for formation control.[12] The problem of maintaining a constellation of satellites in an equally distributed ring formation in earth orbit has been addressed by the behavior-based approach.[13] Ref. [14] also applies this approach to aircraft flying in formation by mimicking group behavior of birds and fish. In ref. [15], a biologically inspired behavior-based method is applied to formation control of unmanned

https://doi.org/10.1017/S0263574707003670 Published online by Cambridge University Press

underwater vehicles (UUV) with the goal of minimizing outside guidance.

Another formation control scheme is the virtual structure approach, in which a group of vehicles acts as a single rigid body.[16] The desired dynamics of the group as a rigid body is defined. Then, the motion of each agent is derived from the trajectory of a corresponding point on the assumed rigid body. Finally, a tracking controller is designed for each agent to track its corresponding trajectory. In this approach, prescribing a coordinated behavior for the group is fairly easy. However, the class of potential applications of this approach is limited because the formation acts as a virtual structure.

In ref. [17], the application of the virtual structure approach to formations of mobile robots is described. This approach was also applied to formations of spacecraft in free space.[18] The virtual structure approach was utilized by naval researchers to design decentralized formation control schemes for a fleet of vessels with a small amount of intervessel communication.[19] An individual parameterized path for each vessel is constructed so that when the parameterization variables are synchronized, the vessels are in formation.

Recently, the research in the area of autonomous aerial vehicles has moved beyond considering a single vehicle. Researchers have considered aerial pursuit/evasion games in three dimensions on a fixed-wing aircraft by implementing and testing a nonlinear model-predictive tracking controller.[20] The pursuit/evasion games has been extended to heterogeneous teams of autonomous agents, in which the problem of having a team of agents pursue a second team of evaders while building a map of the environment has been considered.[21] Another aspect of formation control is formation planning. In formation planning, the initial and final configurations are given for a group of autonomous vehicles, and the nominal input trajectory for each vehicle is determined such that the group can start from the initial configuration and reach its final configuration at a specified time.[22] Another approach to formation control is to introduce carefully designed interagent coupling terms in each performance index of a nonlinear model-predictive controller for the vehicles.[23]

The objective of the current paper is to introduce a new approach for formation control of autonomous helicopters. Formation control of helicopters shares the same challenges with that of other types of vehicles. The need for decentralized controllers, minimum communication, and scalability are among these challenges. The nonlinear dynamics, parameter and model uncertainty, and disturbances add to the common formation control problem difficulties. The current paper contributes to the low-level formation control design for autonomous helicopters, while addressing these difficulties.

The problem of control and coordination for small helicopters moving in a formation is investigated by introducing a leader–follower approach. The overall motion plan for a single virtual lead helicopter is assumed. This motion plan defines the gross motion of the formation. A six-degree-of-freedom (DOF) dynamic model of the helicopters is considered for designing the controllers. It is assumed that four independent actuators control the four control inputs: the main and the tail rotor thrust, and the roll and pitch moments. Two nonlinear decentralized control schemes are required to define a unique three-dimensional formation. In the first scheme, one helicopter controls its relative distance and orientation with respect to a neighboring helicopter. In the second scheme, a helicopter maintains its position in the formation by maintaining specified distances from two neighboring helicopters.

The proposed control schemes only use the state information of the neighboring helicopters. The sliding mode method is used. It is shown that the relative distances and orientations of the helicopters are stabilized even in the presence of wind disturbance. Numerical simulations are presented to demonstrate the efficiency of these techniques.

2. Dynamic Model of a Small Helicopter

This section presents the dynamic model of a helicopter, shown in Fig. 1. Two frames are defined for this dynamic model; the inertial frame {0}, and the helicopter body frame $\{B\}$ with an origin at the center of mass. Six degrees of freedom are assumed for each helicopter. Three translational degrees of freedom, the surge, sway, and bounce of the center of mass, are expressed in the inertial frame {0} and are denoted by $(x^{(0)}, y^{(0)}, z^{(0)})$. Three rotational degrees of freedom are represented by the yaw-pitch-roll (ZYX) Euler angles (ψ, θ, ϕ). These Euler angles define the orientation of the body frame with respect to the inertial frame through the following transformation matrix:[24]

$$\mathbf{R}_{0B} = \begin{bmatrix} \mathrm{c}\psi\,\mathrm{c}\theta & (-\mathrm{s}\psi\,\mathrm{c}\phi & (\mathrm{s}\psi\,\mathrm{s}\phi \\ & +\mathrm{c}\psi\,\mathrm{s}\theta\,\mathrm{s}\phi) & +\mathrm{c}\psi\,\mathrm{s}\theta\,\mathrm{c}\phi) \\ \mathrm{s}\psi\,\mathrm{c}\theta & (\mathrm{c}\psi\,\mathrm{c}\phi & (-\mathrm{c}\psi\,\mathrm{s}\phi \\ & +\mathrm{s}\psi\,\mathrm{s}\theta\,\mathrm{s}\phi) & +\mathrm{s}\psi\,\mathrm{s}\theta\,\mathrm{c}\phi) \\ -\mathrm{s}\theta & \mathrm{c}\theta\,\mathrm{s}\phi & \mathrm{c}\theta\,\mathrm{c}\phi \end{bmatrix} \tag{1}$$

where $\mathrm{c} = \cos$ and $\mathrm{s} = \sin$. The rate of change of the Euler angles are related to the inertial angular velocity vector of the helicopter expressed in the body frame $\boldsymbol{\omega}^{(B)} = [\omega_x^{(B)}, \omega_y^{(B)}, \omega_z^{(B)}]^{\mathrm{T}}$

$$\begin{bmatrix} \dot{\phi} \\ \dot{\theta} \\ \dot{\psi} \end{bmatrix} = \begin{bmatrix} 1 & \sin\phi\tan\theta & \cos\phi\tan\theta \\ 0 & \cos\phi & -\sin\phi \\ 0 & \sin\phi\sec\theta & \cos\phi\sec\theta \end{bmatrix} \boldsymbol{\omega}^{(B).} \tag{2}$$

Although this representation is singular at $\theta = \pm\pi/2$, the helicopter is not expected to operate in that orientation (pointing straight up or down).

The external force and torque expressed in the body frame are $\mathbf{F}^{(B)}$ and $\mathbf{M}^{(B)}$. The external force includes the

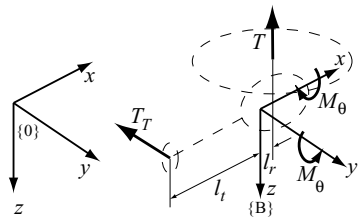

Fig. 1. A six-DOF dynamic model of a helicopter.

https://doi.org/10.1017/S0263574707003670 Published online by Cambridge University Press

aerodynamic drag force vector $\mathbf{D}^{(B)}$, the main and tail rotor thrust T and T_{T}, and the gravitational force mg

$$\mathbf{F}^{(B)} = \mathbf{D}^{(B)} + \begin{bmatrix} 0 \\ -T_{\mathrm{T}} \\ -T \end{bmatrix} + \mathbf{R}_{0B}^{\mathrm{T}} \begin{bmatrix} 0 \\ 0 \\ mg \end{bmatrix}. \tag{3}$$

The external torque includes the three main directional torques M_ϕ, M_θ, and $T_{\mathrm{T}} l_{\mathrm{t}}$ as well as a torque $T l_{\mathrm{r}}$ due to the offset of the rotor hinge with respect to the body z-axis, and the motor torque τ_{m}

$$\mathbf{M}^{(B)} = \begin{bmatrix} M_\phi \\ M_\theta + T l_{\mathrm{r}} \\ T_{\mathrm{T}} l_{\mathrm{t}} + \tau_{\mathrm{m}} \end{bmatrix}. \tag{4}$$

Usually, τ_{m} is assumed to be proportional to the main rotor thrust, T. That is $\tau_{\mathrm{m}} = K_{\mathrm{m}} T$. The translational and rotational equations of motion of the helicopter can be written as

$$m \begin{bmatrix} \ddot{x}^{(0)} \\ \ddot{y}^{(0)} \\ \ddot{z}^{(0)} \end{bmatrix} = \mathbf{R}_{0B} \begin{bmatrix} 0 \\ -T_{\mathrm{T}} \\ -T \end{bmatrix} + \mathbf{R}_{0B} \mathbf{D}^{(B)} + \begin{bmatrix} 0 \\ 0 \\ mg \end{bmatrix} \tag{5}$$

$$\mathbf{I} \begin{bmatrix} \dot{\omega}_x^{(B)} \\ \dot{\omega}_y^{(B)} \\ \dot{\omega}_x^{(B)} \end{bmatrix} = \begin{bmatrix} M_\phi \\ M_\theta + T l_{\mathrm{r}} \\ T_{\mathrm{T}} l_{\mathrm{t}} + \tau_{\mathrm{m}} \end{bmatrix} - \boldsymbol{\omega}^{(B)} \times \mathbf{I} \boldsymbol{\omega}^{(B)} \tag{6}$$

where m is the helicopter mass and $\mathbf{I}$ is:

$$\mathbf{I} = \begin{bmatrix} I_{xx} & 0 & 0 \\ 0 & I_{yy} & 0 \\ 0 & 0 & I_{zz} \end{bmatrix}. \tag{7}$$

The independent inputs that control the helicopter's motion are organized in a column vector

$$\mathbf{u} = [\, T \quad M_\phi \quad M_\theta \quad T_{\mathrm{T}} \,]^{\mathrm{T}}. \tag{8}$$

If the control input $\mathbf{u}$ is known, one can find the trajectory of the helicopter's motion by integrating Eqs. (2), (5), and (6). Our goal is to find a control law that determines $\mathbf{u}$ such that the helicopter follows other helicopters with desired three-dimensional relative distances.

3. Formation Control Schemes

The bulk motion of the group of helicopters can be characterized by trajectory planning and obstacle avoidance algorithms, for example, the method of artificial potential fields. It is assumed that a virtual helicopter as a group leader adapts the bulk motion of the group as its planned trajectory. Other helicopters of the group follow either the virtual group leader or their neighboring helicopters. Therefore, our attention is focused on controlling the internal geometry of the formation. Two types of feedback controllers are introduced for controlling the internal geometry.

The first feedback controller is called the l–α controller. It controls the relative distance and view angle of a helicopter with respect to a neighboring helicopter. This controller is used for helicopters marching in a single file (for example in a line formation) or at an edge of the formation geometry. Note that when the l–α controller is used, a follower can only be related to one leader, which may not be very safe for the formations in which each helicopter is surrounded by more than one helicopter (for example, a rectangular formation). In these situations, forming a triangular formation mesh (Fig. 2) is desirable. The mesh generates a more dense interconnection between the helicopters, which is safer and more robust. To complete a triangular formation mesh, a second controller is needed to control the three-dimensional distances of the helicopter from two neighboring helicopters. This controller is called the l–l controller.

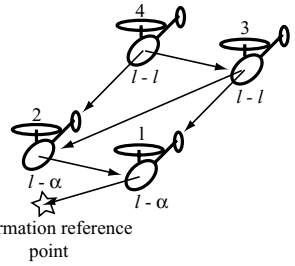

Fig. 2. General formation control configuration.

These two local control schemes can be used to define a solid general formation (Fig. 2). Usually the helicopters at an edge of the formation geometry control their distance with their immediate front helicopter using the l–α controller. The other helicopters control their distances to their immediate front and side helicopters using the l–l controller. This is necessary so that a helicopter can also avoid its side helicopter.

The sliding mode control method is used for deriving low-level control laws for each of the mentioned schemes. Designing a sliding mode control law requires the input–output description of the control system, whereas the equations of motion of the helicopter have been written in state-space form in the previous section. In the next two subsections, the control outputs of the two formation control schemes are defined and the input–output descriptions are derived for the two control systems.

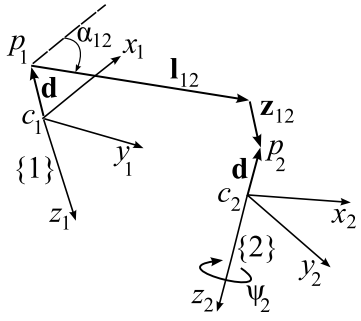

Fig. 3. l–α control configuration. Frames 1 and 2 correspond to the leader and the follower, respectively. The helicopters' centres of mass are denoted by c and their control points are denoted by p.

https://doi.org/10.1017/S0263574707003670 Published online by Cambridge University Press

3.1. Input–output description for the l–α control scheme

In Fig. 3, a system of two neighboring helicopters in the formation is shown. The helicopters are separated by a vectorial distance $\mathbf{l}_{12} + \mathbf{z}_{12}$ between an arbitrary control point, p_1, on helicopter 1 (the leader) and the control point, p_2, on helicopter 2 (the follower). The control point has a fixed distance d with the helicopter center of mass along the negative z-direction of the helicopter's body frame. Note that the helicopters are not physically coupled in any way. A feedback control law for control inputs $\mathbf{u} = [T, M_\phi, M_\theta, T_T]^{\mathrm{T}}$ must be determined to control helicopter 2 such that the desired distance l_{12}^d, view angle α_{12}^d, height offset z_{12}^d, all defined in body frame {1}, to helicopter 1 are maintained, while the yaw angle of helicopter 2, ψ_2^d, follows the yaw angle of helicopter 1. Therefore, the outputs of the control system are: $\mathbf{y} = [l_{12}, \alpha_{12}, z_{12}, \psi_2]^{\mathrm{T}}$.

Here, the input–output description of the control system is derived, which relates the output $\mathbf{y}$ to the input $\mathbf{u}$ directly. First, through a kinematic analysis, the state variables of helicopter 2, which are

$$\mathbf{q}_2 = \left[x_2^{(0)}, y_2^{(0)}, z_2^{(0)}, \dot{x}_2^{(0)}, \dot{y}_2^{(0)}, \dot{z}_2^{(0)}, \phi_2, \theta_2, \psi_2, \omega_{2x}^{(2)}, \omega_{2y}^{(2)}, \omega_{2x}^{(2)}\right]^T \tag{9}$$

are related to the output $\mathbf{y}$. Then, the equations of motion, containing $\mathbf{u}$ are substituted in the resulting equations to give the input–output relations. The details follow.

3.1.1. Kinematic analysis. Let us consider the moving body frames of helicopters 1 and 2 (Fig. 3). We assume two coincident points; point p_2', attached to frame {1}, and point p_2, attached to frame {2}, both coincident with the instantaneous location of the follower's control point. If $\mathbf{v}_{p2/1}^{(1)}$ and $\mathbf{a}_{p2/1}^{(1)}$ are the apparent velocity and acceleration of point p_2 as seen by an observer at point p_2' attached to frame {1} expressed in {1}, one can write

$$\mathbf{v}_{p2/1}^{(1)} = (\dot{\mathbf{l}}_{12} + \dot{\mathbf{z}}_{12}) \tag{10}$$

$$\mathbf{a}_{p2/1}^{(1)} = (\ddot{\mathbf{l}}_{12} + \ddot{\mathbf{z}}_{12}). \tag{11}$$

If $\mathbf{a}_{p2/1}^{c(1)}$ is the Coriolis acceleration of the point p_2 as seen by an observer at point p_2' expressed in {1}, one can write

$$\mathbf{a}_{p2}^{(1)} = \mathbf{a}_{p\prime 2}^{(1)} + \mathbf{a}_{p2/1}^{c(1)} + \mathbf{a}_{p2/1}^{(1)} \tag{12}$$

where

$$\mathbf{a}_{p\prime 2}^{(1)} = \mathbf{a}_{p1}^{(1)} + \dot{\boldsymbol{\omega}}_1^{(1)} \times (\mathbf{l}_{12} + \mathbf{z}_{12}) + \boldsymbol{\omega}_1^{(1)} \times \left(\boldsymbol{\omega}_1^{(1)} \times (\mathbf{l}_{12} + \mathbf{z}_{12})\right) \tag{13}$$

$$\mathbf{a}_{p1}^{(1)} = \mathbf{R}_{01}^{\mathrm{T}}\left(\ddot{x}_1^{(0)}\hat{\mathbf{i}}_0 + \ddot{y}_1^{(0)}\hat{\mathbf{j}}_0 + \ddot{z}_1^{(0)}\hat{\mathbf{k}}_0\right) + \boldsymbol{\omega}_1^{(1)} \times \mathbf{d}^{(1)} \tag{14}$$

$$\mathbf{a}_{p2/1}^{c(1)} = 2\boldsymbol{\omega}_1^{(1)} \times \mathbf{v}_{p2/1}^{(1)}. \tag{15}$$

After combining these relations, the absolute acceleration of the control point p_2 becomes

$$\mathbf{a}_{p2}^{(1)} = \mathbf{R}_{01}^{\mathrm{T}}\mathbf{a}_{p1}^{(0)} + \dot{\boldsymbol{\omega}}_1^{(1)} \times (\mathbf{l}_{12} + \mathbf{z}_{12}) + \boldsymbol{\omega}_1^{(1)} \times \left(\boldsymbol{\omega}_1^{(1)} \times (\mathbf{l}_{12} + \mathbf{z}_{12})\right) + 2\boldsymbol{\omega}_1^{(1)} \times \mathbf{v}_{p2/1}^{(1)} + (\ddot{\mathbf{l}}_{12} + \ddot{\mathbf{z}}_{12}). \tag{16}$$

On the other hand, the acceleration of the same point p_2 can be calculated in terms of the absolute acceleration of the center of mass of helicopter 2 as

$$\mathbf{a}_{p2}^{(1)} = \mathbf{R}_{01}^{\mathrm{T}}\mathbf{R}_{02}\left(\mathbf{a}_{c2}^{(2)} + \dot{\boldsymbol{\omega}}_2^{(2)} \times \mathbf{d}^{(2)} + \boldsymbol{\omega}_2^{(2)} \times \left(\boldsymbol{\omega}_2^{(2)} \times \mathbf{d}^{(2)}\right)\right) \tag{17}$$

where

$$\mathbf{a}_{c2}^{(2)} = \mathbf{R}_{02}^{\mathrm{T}}\left(\ddot{x}_2^{(0)}\hat{\mathbf{i}}_0 + \ddot{y}_2^{(0)}\hat{\mathbf{j}}_0 + \ddot{z}_2^{(0)}\hat{\mathbf{k}}_0\right) \tag{18}$$

$$\mathbf{d}^{(2)} = -d\hat{\mathbf{k}}_2. \tag{19}$$

The absolute acceleration of point p_2 must be the same, independent of how it is calculated. Therefore, one can equate Eqs. (16) and (17). By solving the resulting vectorial equation for $\ddot{\mathbf{l}}_{12} + \ddot{\mathbf{z}}_{12}$, one can obtain the following vectorial kinematic equation:

$$(\ddot{\mathbf{l}}_{12} + \ddot{\mathbf{z}}_{12}) = \mathbf{R}_{01}^{\mathrm{T}}\left[\mathbf{a}_{c2}^{(0)} + \mathbf{R}_{02}\left(\dot{\boldsymbol{\omega}}_2^{(2)} \times \mathbf{d}^{(2)}\right)\right] + \mathbf{B}_0 \tag{20}$$

where

$$\mathbf{B}_0 = \mathbf{R}_{01}^{\mathrm{T}}\left[-\mathbf{a}_{p1}^{(0)} + \mathbf{R}_{02}\left(\boldsymbol{\omega}_2^{(2)} \times \left(\boldsymbol{\omega}_2^{(2)} \times \mathbf{d}^{(2)}\right)\right)\right] - \dot{\boldsymbol{\omega}}_1^{(1)} \times (\mathbf{l}_{12} + \mathbf{z}_{12}) - \boldsymbol{\omega}_1^{(1)} \times \left(\boldsymbol{\omega}_1^{(1)} \times (\mathbf{l}_{12} + \mathbf{z}_{12})\right) - 2\boldsymbol{\omega}_1^{(1)} \times (\dot{\mathbf{l}}_{12} + \dot{\mathbf{z}}_{12}). \tag{21}$$

Since $\mathbf{l}_{12} + \mathbf{z}_{12} = [l_{12}\,\mathrm{c}\alpha_{12}, l_{12}\,\mathrm{s}\alpha_{12}, z_{12}]^{\mathrm{T}}$, the left-hand side of Eq. (20) can be expanded as

$$(\ddot{\mathbf{l}}_{12} + \ddot{\mathbf{z}}_{12}) = \mathbf{A}_1\ddot{\mathbf{y}}_1 + \mathbf{B}_1 \tag{22}$$

in which

$$\mathbf{A}_1 = \begin{bmatrix} \mathrm{c}\alpha_{12} & -l_{12}\,\mathrm{s}\alpha_{12} & 0 \\ \mathrm{s}\alpha_{12} & l_{12}\,\mathrm{c}\alpha_{12} & 0 \\ 0 & 0 & 1 \end{bmatrix}, \qquad \mathbf{y}_1 = \begin{bmatrix} l_{12} \\ \alpha_{12} \\ z_{12} \end{bmatrix},$$

$$\mathbf{B}_1 = \begin{bmatrix} -2\dot{l}_{12}\dot{\alpha}_{12}\mathrm{s}\alpha_{12} - l_{12}\dot{\alpha}_{12}^2\,\mathrm{c}\alpha_{12} \\ 2\dot{l}_{12}\dot{\alpha}_{12}\,\mathrm{c}\alpha_{12} - l_{12}\dot{\alpha}_{12}^2\,\mathrm{s}\alpha_{12} \\ 0 \end{bmatrix}. \tag{23}$$

By combining Eqs. (20) and (22), one can arrive at an equation that relates a subset of the output vector, $\mathbf{y}_1$, to the state variables of the helicopters

$$\ddot{\mathbf{y}}_1 = \mathbf{A}_1^{-1}\left[\mathbf{R}_{01}^{\mathrm{T}}\left[\mathbf{a}_{c2}^{(0)} + \mathbf{R}_{02}\left(\dot{\boldsymbol{\omega}}_2^{(2)} \times \mathbf{d}^{(2)}\right)\right] + \mathbf{B}_0 - \mathbf{B}_1\right]. \tag{24}$$

Note that $\mathbf{A}_1$ is invertible as long as $l_{12} \neq 0$, which can be easily avoided by defining an appropriate desired formation.

https://doi.org/10.1017/S0263574707003670 Published online by Cambridge University Press

3.1.2. Input–output equations. The linear and angular accelerations of helicopter 2, the follower, appear in Eq. (24). In this subsection, first, these accelerations are substituted by the dynamic equations of helicopter 2, which include the inputs, to give a subset of the input–output equations. Then, the input–output equations are completed by including the dynamics of the follower's yaw-degree-of-freedom, ψ_2.

The translational dynamic equation (5) is customized for helicopter 2 by adding an index 2 to the variables and noting that the body-frame notation $\{B\}$ is replaced by notion $\{2\}$. The resulting dynamic equation can be rearranged and written in the following matrix form

$$\mathbf{a}_{c2}^{(0)} = \mathbf{C}_1\mathbf{u} + \mathbf{D}_1 + \mathbf{W}_1 \tag{25}$$

where

$$\mathbf{C}_1 = \frac{1}{m}\mathbf{R}_{02}\begin{bmatrix} 0 & 0 & 0 & 0 \\ 0 & 0 & 0 & -1 \\ -1 & 0 & 0 & 0 \end{bmatrix},$$

$$\mathbf{D}_1 = \frac{1}{m}\mathbf{R}_{02}\mathbf{D}^{(2)}, \quad \mathbf{W}_1 = \begin{bmatrix} 0 \\ 0 \\ g \end{bmatrix}. \tag{26}$$

Also, the term $(\dot{\boldsymbol{\omega}}_2^{(2)} \times \mathbf{d}^{(2)})$ is derived by customizing the rotational equation of motion (6) for helicopter 2 and calculating the cross product. This results in

$$\dot{\boldsymbol{\omega}}_2^{(2)} \times \mathbf{d}^{(2)} = \mathbf{C}_2\mathbf{u} + \mathbf{D}_2 \tag{27}$$

where

$$\mathbf{C}_2 = \begin{bmatrix} -\frac{dl_r}{I_{yy}} & 0 & -\frac{d}{I_{yy}} & 0 \\ 0 & \frac{d}{I_{xx}} & 0 & 0 \\ 0 & 0 & 0 & 0 \end{bmatrix}$$

$$\mathbf{D}_2 = -\left[\mathbf{I}^{-1}\left(\boldsymbol{\omega}_2^{(2)} \times \mathbf{I}\boldsymbol{\omega}_2^{(2)}\right)\right] \times \mathbf{d}^{(2)}. \tag{28}$$

Now, a subset of the required input–output equations can be obtained by substituting Eqs. (25) and (27) into Eq. (24)

$$\ddot{\mathbf{y}}_1 = \mathbf{f}_1 + \mathbf{b}_1\mathbf{u} \tag{29}$$

where

$$\mathbf{f}_1 = \mathbf{A}_1^{-1}\left[\mathbf{R}_{01}^{\mathrm{T}}(\mathbf{W}_1 + \mathbf{R}_{02}\mathbf{D}_2) + \mathbf{B}_0 - \mathbf{B}_1 + \mathbf{R}_{01}^{\mathrm{T}}\mathbf{D}_1\right]$$
$$\mathbf{b}_1 = \mathbf{A}_1^{-1}\left[\mathbf{R}_{01}^{\mathrm{T}}(\mathbf{C}_1 + \mathbf{R}_{02}\mathbf{C}_2)\right]. \tag{30}$$

Note that the yaw angle of helicopter 2 (ψ_2) as the last output component is missing from this subset of input–output equations, because $\mathbf{y}_1$ contains only the three outputs l_{12}, α_{12}, and z_{12}. This component must also be included in the input–output equations. The dynamics of the yaw angle is derived by differentiating the third component of Eq. (2). The result of this differentiation takes the following standard matrix form:

$$\ddot{\psi}_2 = f_2 + \mathbf{b}_2\mathbf{u} \tag{31}$$

where

$$\begin{aligned} f_2 = {} & (\dot{\phi}_2 \cos\phi_2 \sec\theta_2 + \dot{\theta}_2 \sin\phi_2 \sec\theta_2 \tan\theta_2)\omega_{2y}^{(2)} \\ & + (-\dot{\phi}_2 \sin\phi_2 \sec\theta_2 + \dot{\theta}_2 \cos\phi_2 \sec\theta_2 \tan\theta_2)\omega_{2z}^{(2)} \\ & + (\sin\phi_2 \sec\theta_2)\left((I_{zz} - I_{xx})\omega_{2x}^{(2)}\omega_{2z}^{(2)}/I_{yy}\right) \\ & + (\cos\phi_2 \sec\theta_2)\left((I_{xx} - I_{yy})\omega_{2x}^{(2)}\omega_{2y}^{(2)}/I_{zz}\right) \end{aligned} \tag{32}$$

$$\begin{aligned} \mathbf{b}_2 = {} & \left[\frac{\sin\phi_2 \sec\theta_2 l_r}{I_{yy}} - \frac{\cos\phi_2 \sec\theta_2 K_m}{I_{zz}}, 0,\right. \\ & \left.\frac{\sin\phi_2 \sec\theta_2}{I_{yy}}, \frac{\cos\phi_2 \sec\theta_2}{I_{zz}}\right] \end{aligned} \tag{33}$$

The full set of input–output equations are obtained by combining Eqs. (29) and (31) into a single matrix form:

$$\begin{bmatrix} \ddot{l}_{12} \\ \ddot{\alpha}_{12} \\ \ddot{z}_{12} \\ \hline \ddot{\psi}_2 \end{bmatrix} = \begin{bmatrix} \mathbf{f}_{1(3\times1)} \\ \hline f_2 \end{bmatrix} + \begin{bmatrix} \mathbf{b}_{1(3\times4)} \\ \hline \mathbf{b}_{2(1\times4)} \end{bmatrix} \begin{bmatrix} T \\ M_\phi \\ M_\theta \\ T_{\mathrm{T}} \end{bmatrix} \tag{34}$$

or in a more concise form

$$\ddot{\mathbf{y}} = \mathbf{f} + \mathbf{b}\mathbf{u}. \tag{35}$$

3.2. Input–output description for the l–l control scheme

In Fig. 4, a system of three neighboring helicopters in the formation is shown. The control point of the follower helicopter, p_3, is separated from the control points of leader 1 and leader 2, p_1 and p_2, by two three-dimensional vectorial distances $\mathbf{l}_{13}$ and $\mathbf{l}_{23}$, respectively. The formation plane $p_1p_2p_3$ makes an angle of β_{123} with a reference direction (Fig. 5). Note that the helicopters are not physically coupled in any way. A feedback control law for control inputs

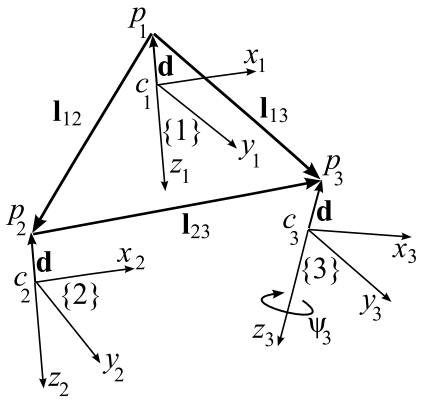

Fig. 4. *l–l* control configuration. Frames 1–3 correspond to the first leader, the second leader, and the follower, respectively. The helicopters' centres of mass are denoted by c and their control points are denoted by p.

https://doi.org/10.1017/S0263574707003670 Published online by Cambridge University Press

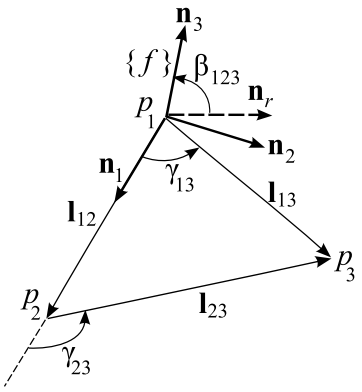

Fig. 5. Definition of the formation frame for the *l–l* control scheme. The three helicopters' control points are denoted by p_1–p_3. Unit vector $\mathbf{n}_1$ points from p_1 to p_2. Unit vector $\mathbf{n}_3$ is perpendicular to the formation plane $p_1p_2p_3$. Unit vector $\mathbf{n}_2$ lies in the formation plane and makes a right-hand frame $\{f\}$ with $\mathbf{n}_1$ and $\mathbf{n}_3$. The frame $\{f\}$ is called the formation frame. Unit vector $\mathbf{n}_r$ lies in the global horizontal plane and is perpendicular to $\mathbf{n}_1$. When the formation plane is horizontal, $\beta_{123} = \frac{\pi}{2}$.

$\mathbf{u} = [T, M_\phi, M_\theta, T_T]^T$ must be determined to control helicopter 3 such that the desired distances l_{13}^d, l_{23}^d, and angle β_{123}^d are maintained, while the yaw angle of helicopter 3, ψ_3, follows a desired trajectory. With these definitions, the outputs of the control system are: $\mathbf{y} = [l_{13}, l_{23}, \beta_{123}, \psi_3]^T$.

Here, the input–output description of the control system are derived, which relate the output $\mathbf{y}$ to the input $\mathbf{u}$ directly. First, through a kinematic analysis, the state variables of helicopter 3

$$\mathbf{q}_3 = \left[x_3^{(0)}, y_3^{(0)}, z_3^{(0)}, \dot{x}_3^{(0)}, \dot{y}_3^{(0)}, \dot{z}_3^{(0)} \phi_3, \theta_3, \psi_3, \omega_{3x}^{(3)}, \omega_{3y}^{(3)}, \omega_{3x}^{(3)}\right]^T \tag{36}$$

are related to the output $\mathbf{y}$. Then, the equations of motion, containing $\mathbf{u}$ are substituted in the resulting equations to give the input–output relations. The details follow.

3.2.1. Kinematic analysis. The control points of the three helicopters in an *l–l* scheme form a three-dimensional plane (the formation plane). The plane of formation $p_1p_2p_3$ and its local coordinate frame $\{f\}$ are shown in Fig. 5. Since the unit vectors of the coordinate frame $\{f\}$ are defined based on the location of the three helicopters, this frame moves and rotates when the three helicopters move. The angular velocity and acceleration of this frame is required for calculating the rate of change of the formation parameters (control outputs) defined in the previous section. In the following, first, the formation frame is defined. Then, the angular velocity and acceleration of this frame are determined. And finally, the rate of change of the formation parameters (control outputs) are calculated.

The mutually perpendicular unit vectors of the formation frame $\{f\}$, whose origin is at p_1, are defined as

$$\mathbf{n}_1 = \frac{\mathbf{l}_{12}}{|\mathbf{l}_{12}|}, \quad \mathbf{n}_3 = \frac{\mathbf{l}_{12} \times \mathbf{l}_{13}}{|\mathbf{l}_{12} \times \mathbf{l}_{13}|}, \quad \mathbf{n}_2 = \mathbf{n}_3 \times \mathbf{n}_1. \tag{37}$$

A reference $\mathbf{n}_r$ for rotation of the formation plane about $\mathbf{l}_{12}$ is needed to define the formation parameter β_{123}. This reference unit vector is assumed to lie in the global horizontal plane and be perpendicular to $\mathbf{l}_{12}$. It is calculated as

$$\mathbf{n}_r = \frac{\mathbf{l}_{12} \times \mathbf{k}_0}{|\mathbf{l}_{12} \times \mathbf{k}_0|}. \tag{38}$$

Now, the rotation of the formation plane about $\mathbf{l}_{12}$ in reference to $\mathbf{n}_r$, which is one of the formation parameters, is defined as

$$\beta_{123} = \arccos(\mathbf{n}_r \cdot \mathbf{n}_3). \tag{39}$$

The angular velocity of the formation frame is defined as

$$\boldsymbol{\omega}_f^{(f)} = \dot{\beta}_{123}\mathbf{n}_1 + \omega_{f2}\mathbf{n}_2 + \omega_{f3}\mathbf{n}_3. \tag{40}$$

The second and third components of $\boldsymbol{\omega}_f^{(f)}$ can be found by observing the relative velocity of points p_1 and p_2

$$\mathbf{v}_{p2}^{(f)} = \mathbf{v}_{p1}^{(f)} + \boldsymbol{\omega}_f^{(f)} \times \mathbf{l}_{12}^{(f)} + \dot{\mathbf{l}}_{12}^{(f)} \tag{41}$$

where $\mathbf{l}_{12}^{(f)} = l_{12}\mathbf{n}_1$ and $\dot{\mathbf{l}}_{12}^{(f)} = \dot{l}_{12}\mathbf{n}_1$. Two of the three components of $\boldsymbol{\omega}_f^{(f)}$ can be obtained by rearranging Eq. (41) as

$$\begin{bmatrix} \dot{l}_{12} \\ l_{12}\omega_{f3} \\ -l_{12}\omega_{f2} \end{bmatrix} = \mathbf{R}_{0f}^T\left(\mathbf{v}_{p2}^{(0)} - \mathbf{v}_{p1}^{(0)}\right). \tag{42}$$

The first component of $\boldsymbol{\omega}_f^{(f)}$ is found by writing a relative velocity equation between points p_1 and p_3

$$\mathbf{v}_{p3}^{(f)} = \mathbf{v}_{p1}^{(f)} + \boldsymbol{\omega}_f^{(f)} \times \mathbf{l}_{13}^{(f)} + \dot{\mathbf{l}}_{13}^{(f)} \tag{43}$$

where $\mathbf{l}_{13}^{(f)} = l_{13}(\cos\gamma_{13}\mathbf{n}_1 + \sin\gamma_{13}\mathbf{n}_2)$ and $\dot{\mathbf{l}}_{13}^{(f)} = \dot{l}_{13}(\cos\gamma_{13}\mathbf{n}_1 + \sin\gamma_{13}\mathbf{n}_2)$, as concluded from Fig. 5. $\dot{\beta}_{123}$ can be found by simplifying the third component of Eq. (43)

$$\dot{\beta}_{123} = \frac{v_{p3z}^{(f)} - v_{p1z}^{(f)} + \omega_{f2}l_{13}\cos\gamma_{13}}{l_{13}\sin\gamma_{13}}. \tag{44}$$

$\dot{\beta}_{123}$ can be calculated as long as l_{13} and γ_{13} are nonzero. These situations can be avoided when defining the desired formation parameters. $l_{13}^d = 0$ means that the helicopters are coincident, which is physically impossible, and must not be used. $\gamma_{13}^d = 0$ corresponds to the situation when the three helicopters' control points are on the same line. In this situation, two *l–α* schemes must be used to define the desired formation. Note that if the control points p_2 and p_3 are used for finding the rate $\dot{\beta}_{123}$, the same result will be obtained (Appendix A1).

The angular acceleration of the formation frame, $\dot{\boldsymbol{\omega}}_f^{(f)}$, is also required for deriving the input–output equations of the *l–l* control scheme. Two components of this acceleration can be obtained by observing the relative acceleration of points

https://doi.org/10.1017/S0263574707003670 Published online by Cambridge University Press

p_1 and p_2

$$\mathbf{a}_{p2}^{(f)} = \mathbf{a}_{p1}^{(f)} + \dot{\boldsymbol{\omega}}_f^{(f)} \times \mathbf{l}_{12}^{(f)} + \boldsymbol{\omega}_f^{(f)} \times \left(\boldsymbol{\omega}_f^{(f)} \times \mathbf{l}_{12}^{(f)}\right) + 2\boldsymbol{\omega}_f^{(f)} \times \dot{\mathbf{l}}_{12}^{(f)} + \ddot{\mathbf{l}}_{12}^{(f)} \tag{45}$$

where $\ddot{\mathbf{l}}_{12}^{(f)} = \ddot{l}_{12}\mathbf{n}_1$ and $\dot{\boldsymbol{\omega}}_f^{(f)} = \ddot{\beta}_{123}\mathbf{n}_1 + \alpha_{f2}\mathbf{n}_2 + \alpha_{f3}\mathbf{n}_3$. The second and third components of the formation-frame angular acceleration are obtained by rearranging Eq. (45)

$$\begin{bmatrix} \ddot{l}_{12} \\ l_{12}\alpha_{f3} \\ -l_{12}\alpha_{f2} \end{bmatrix} = \mathbf{R}_{0f}^T\left(\mathbf{a}_{p2}^{(0)} - \mathbf{a}_{p1}^{(0)}\right) - \boldsymbol{\omega}_f^{(f)} \times \left(\boldsymbol{\omega}_f^{(f)} \times \mathbf{l}_{12}^{(f)}\right) - 2\boldsymbol{\omega}_f^{(f)} \times \dot{\mathbf{l}}_{12}^{(f)}. \tag{46}$$

After the angular motion of the formation frame is known, the rate of change of the formation parameters l_{13}, l_{23}, and β_{123} can be determined by investigating the relative motion of point p_3 with respect to points p_1 and p_2 separately. This is first shown by considering the relative motion of point p_3 with respect to p_1 to obtain $\ddot{l}_{13}$ and $\ddot{\beta}_{123}$. Then, the results are simply extended for $\ddot{l}_{23}$. The acceleration of p_3 can be formulated as

$$\mathbf{a}_{p3}^{(f)} = \mathbf{a}_{p1}^{(f)} + \dot{\boldsymbol{\omega}}_f^{(f)} \times \mathbf{l}_{13}^{(f)} + \boldsymbol{\omega}_f^{(f)} \times \left(\boldsymbol{\omega}_f^{(f)} \times \mathbf{l}_{13}^{(f)}\right) + 2\boldsymbol{\omega}_f^{(f)} \times \dot{\mathbf{l}}_{13}^{(f)} + \ddot{\mathbf{l}}_{13}^{(f)}. \tag{47}$$

On the other hand, the same acceleration can be derived with respect to the follower's center of mass c_3.

$$\mathbf{a}_{p3}^{(f)} = \mathbf{a}_{c3}^{(f)} + \dot{\boldsymbol{\omega}}_3^{(f)} \times \mathbf{d}^{(f)} + \boldsymbol{\omega}_3^{(f)} \times \left(\boldsymbol{\omega}_3^{(f)} \times \mathbf{d}^{(f)}\right). \tag{48}$$

Combining Eqs. (47) and (48) and defining the terms

$$\mathbf{N}_1 = \boldsymbol{\omega}_3^{(f)} \times \left(\boldsymbol{\omega}_3^{(f)} \times \mathbf{d}^{(f)}\right) - \mathbf{a}_{p1}^{(f)} - \boldsymbol{\omega}_f^{(f)} \times \left(\boldsymbol{\omega}_f^{(f)} \times \mathbf{l}_{12}^{(f)}\right) - 2\boldsymbol{\omega}_f^{(f)} \times \dot{\mathbf{l}}_{12}^{(f)} \tag{49}$$

$$\mathbf{M}_1 = [\,0 \quad 0 \quad -\alpha_{f2} l_{13} \cos\gamma_{13}\,]^{\mathrm{T}} \tag{50}$$

results in

$$\begin{bmatrix} \ddot{l}_{13}\cos\gamma_{13} - \alpha_{f3} l_{13}\sin\gamma_{13} \\ \ddot{l}_{13}\sin\gamma_{13} + \alpha_{f3} l_{13}\cos\gamma_{13} \\ \ddot{\beta}_{123} l_{13}\sin\gamma_{13} \end{bmatrix} = \mathbf{a}_{c3}^{(f)} + \dot{\boldsymbol{\omega}}_3^{(f)} \times \mathbf{d}^{(f)} + \mathbf{N}_1 - \mathbf{M}_1. \tag{51}$$

Equation (51) can be further simplified to obtain $\ddot{l}_{13}$ and $\ddot{\beta}_{123}$

$$\begin{bmatrix} \ddot{l}_{13} \\ l_{13}\alpha_{f3} \\ \ddot{\beta}_{123} \end{bmatrix} = \mathbf{A}_3^{-1}\left(\mathbf{a}_{c3}^{(f)} + \dot{\boldsymbol{\omega}}_3^{(f)} \times \mathbf{d}^{(f)} + \mathbf{N}_1 - \mathbf{M}_1\right) \tag{52}$$

where

$$\mathbf{A}_3 = \begin{bmatrix} \cos\gamma_{13} & -\sin\gamma_{13} & 0 \\ \sin\gamma_{13} & \cos\gamma_{13} & 0 \\ 0 & 0 & l_{13}\sin\gamma_{13} \end{bmatrix}. \tag{53}$$

This matrix is invertible as long as l_{13} and γ_{13} are nonzero.

The rate of change for l_{23} can be obtained with the same procedure as mentioned earlier. The result is

$$\begin{bmatrix} \ddot{l}_{23} \\ l_{23}\alpha_{f3} \\ \ddot{\beta}_{123} \end{bmatrix} = \mathbf{A}_4^{-1}\left(\mathbf{a}_{c3}^{(f)} + \dot{\boldsymbol{\omega}}_3^{(f)} \times \mathbf{d}^{(f)} + \mathbf{N}_2 - \mathbf{M}_2\right) \tag{54}$$

where

$$\mathbf{A}_4 = \begin{bmatrix} \cos\gamma_{23} & -\sin\gamma_{23} & 0 \\ \sin\gamma_{23} & \cos\gamma_{23} & 0 \\ 0 & 0 & l_{23}\sin\gamma_{23} \end{bmatrix} \tag{55}$$

$$\mathbf{N}_2 = \boldsymbol{\omega}_3^{(f)} \times \left(\boldsymbol{\omega}_3^{(f)} \times \mathbf{d}^{(f)}\right) - \mathbf{a}_{p2}^{(f)} - \boldsymbol{\omega}_f^{(f)} \times \left(\boldsymbol{\omega}_f^{(f)} \times \mathbf{l}_{23}^{(f)}\right) - 2\boldsymbol{\omega}_f^{(f)} \times \dot{\mathbf{l}}_{23}^{(f)} \tag{56}$$

$$\mathbf{M}_2 = [\,0 \quad 0 \quad -\alpha_{f2} l_{23}\cos\gamma_{23}\,]^{\mathrm{T}}. \tag{57}$$

$\mathbf{A}_4$ can be inverted as long as l_{23} and γ_{23} are nonzero. These situations can be avoided when defining the desired formation parameters. $l_{23}^d = 0$ means that the helicopters are coincident, which is physically impossible and must not be used. $\gamma_{23}^d = 0$ corresponds to the situation when the three helicopters' control points are on the same line. In this situation, two l–α schemes must be used to define the desired formation.

It can be shown that the result for $\ddot{\beta}_{123}$ from Eq. (54) is equal to the result obtained in Eq. (52) (Appendix A2). Now, a subset of the output vector $\mathbf{y}_2 = [l_{13}, l_{23}, \beta_{123}]^{\mathrm{T}}$ can be formed by combining Eqs. (52) and (54) as follows

$$\ddot{\mathbf{y}}_2 = \begin{bmatrix} \ddot{l}_{13} \\ \ddot{l}_{23} \\ \ddot{\beta}_{123} \end{bmatrix} = \mathbf{C}_3 \begin{bmatrix} \ddot{l}_{13} \\ l_{13}\alpha_{f3} \\ \ddot{\beta}_{123} \end{bmatrix} + \mathbf{C}_4 \begin{bmatrix} \ddot{l}_{23} \\ l_{23}\alpha_{f3} \\ \ddot{\beta}_{123} \end{bmatrix} \tag{58}$$

where

$$\mathbf{C}_3 = \begin{bmatrix} 1 & 0 & 0 \\ 0 & 0 & 0 \\ 0 & 0 & 1 \end{bmatrix} \quad \mathbf{C}_4 = \begin{bmatrix} 0 & 0 & 0 \\ 1 & 0 & 0 \\ 0 & 0 & 0 \end{bmatrix}. \tag{59}$$

3.2.2. Input–output equations. Part of the input–output description of the l–l control scheme is derived by substituting Eqs. (52) and (54) into Eq. (58)

$$\ddot{\mathbf{y}}_2 = \left(\mathbf{C}_3\mathbf{A}_3^{-1} + \mathbf{C}_4\mathbf{A}_4^{-1}\right)\left(\mathbf{a}_{c3}^{(f)} + \dot{\boldsymbol{\omega}}_3^{(f)} \times \mathbf{d}^{(f)}\right) + \mathbf{C}_3\mathbf{A}_3^{-1}(\mathbf{N}_1 - \mathbf{M}_1) + \mathbf{C}_4\mathbf{A}_4^{-1}(\mathbf{N}_2 - \mathbf{M}_2). \tag{60}$$

https://doi.org/10.1017/S0263574707003670 Published online by Cambridge University Press

This part of the input–output description is completed by using frame conversions

$$\mathbf{a}_{c3}^{(f)} = \mathbf{R}_{0f}^{\mathrm{T}}\mathbf{a}_{c3}^{(0)}, \quad \dot{\boldsymbol{\omega}}_3^{(f)} \times \mathbf{d}^{(f)} = \mathbf{R}_{0f}^{\mathrm{T}}\mathbf{R}_{03}\big(\dot{\boldsymbol{\omega}}_3^{(3)} \times \mathbf{d}^{(3)}\big) \quad (61)$$

and substituting for $\mathbf{a}_{c3}^{(0)}$ and $\dot{\boldsymbol{\omega}}_3^{(3)} \times \mathbf{d}^{(3)}$ using equations similar to Eqs. (25) and (27) for the dynamics of the follower. The result can be rearranged as

$$\ddot{\mathbf{y}}_2 = \mathbf{f}_3 + \mathbf{b}_3\mathbf{u} \quad (62)$$

where

$$\mathbf{b}_3 = \big(\mathbf{C}_3\mathbf{A}_3^{-1} + \mathbf{C}_4\mathbf{A}_4^{-1}\big)\big(\mathbf{R}_{0f}^{\mathrm{T}}\mathbf{C}_1 + \mathbf{R}_{0f}^{\mathrm{T}}\mathbf{R}_{03}\mathbf{C}_2\big) \quad (63)$$

$$\mathbf{f}_3 = \big(\mathbf{C}_3\mathbf{A}_3^{-1} + \mathbf{C}_4\mathbf{A}_4^{-1}\big)\big(\mathbf{R}_{0f}^{\mathrm{T}}(\mathbf{D}_1 + \mathbf{W}_1) + \mathbf{R}_{0f}^{\mathrm{T}}\mathbf{R}_{03}\mathbf{D}_2\big) + \mathbf{C}_3\mathbf{A}_3^{-1}(\mathbf{N}_1 - \mathbf{M}_1) + \mathbf{C}_4\mathbf{A}_4^{-1}(\mathbf{N}_2 - \mathbf{M}_2) \quad (64)$$

The full set of input–output equations are obtained by augmenting the yaw dynamics $\ddot{\psi}_3$ of the follower as the fourth formation parameter with Eq. (62). Relations similar to Eqs. (31)–(33) can be used, in which the subscript 2 for the follower states is replaced by 3 indicating the use of the follower 3 states.

$$\ddot{\psi}_3 = f_4 + \mathbf{b}_4\mathbf{u}. \quad (65)$$

This results in a single-matrix form for the l–l input–output description

$$\begin{bmatrix} \ddot{l}_{13} \\ \ddot{l}_{23} \\ \ddot{\beta}_{123} \\ \hline \ddot{\psi}_3 \end{bmatrix} = \begin{bmatrix} \mathbf{f}_{3(3\times1)} \\ \hline f_4 \end{bmatrix} + \begin{bmatrix} \mathbf{b}_{3(3\times4)} \\ \hline \mathbf{b}_{4(1\times4)} \end{bmatrix} \begin{bmatrix} T \\ M_\phi \\ M_\theta \\ T_T \end{bmatrix} \quad (66)$$

or in a more concise form

$$\ddot{\mathbf{y}} = \mathbf{f} + \mathbf{b}\mathbf{u}. \quad (67)$$

4. Designing the Sliding-Mode Control Law

In the previous sections, the input–output description for both the l–α and l–l control schemes were derived. They were written in a similar general matrix form [Eqs. (35) and (67)] to simplify the control law development. The sliding-mode control method is used to design a controller based on the matrix form of the input–output equations. In this method, four first-order asymptotically stable surface functions are assumed[25]

$$\mathbf{s} = (\dot{\mathbf{y}} - \dot{\mathbf{y}}^d) + \boldsymbol{\lambda}(\mathbf{y} - \mathbf{y}^d) \quad (68)$$

where $\boldsymbol{\lambda} = \mathrm{diag}(\lambda_1, \lambda_2, \lambda_3, \lambda_4)$, and all λ's are positive. Equation (68) is written in the following form for convenience

$$\mathbf{s} = \dot{\mathbf{y}} - \mathbf{s}_{\mathrm{r}} \quad (69)$$

where

$$\mathbf{s}_{\mathrm{r}} = \dot{\mathbf{y}}^d - \boldsymbol{\lambda}(\mathbf{y} - \mathbf{y}^d). \quad (70)$$

If the trajectory of the system can be controlled such that $\mathbf{s}$ approaches zero and remains zero at all times, since the surface (68) is asymptotically stable, it is guaranteed that the output $\mathbf{y}$ converges to its desired value. Therefore, the sliding-mode controller design reduces to finding a control law that brings and keeps the output of the system on the sliding surface. The following Lyaponuv function is defined for the components of $\mathbf{s}$

$$\dot{s}_i \cdot s_i \le 0, \qquad i = 1, \ldots, 4 \quad (71)$$

If the dynamics of $\mathbf{s}$ is selected as

$$\dot{s}_i = -k_i\ \mathrm{sgn}(s_i), \qquad i = 1, \ldots, 4 \quad (72)$$

where $k_i > 0$, the Lyaponuv function (71) is satisfied and it is guaranteed that the trajectory of the outputs approach the surface $\mathbf{s}$ and remain on the surface. After selecting the dynamics of $\mathbf{s}$, the control inputs must be determined such that they actually create this dynamics. This is done by differentiating Eq. (69), substituting the input–output description (67) for $\ddot{\mathbf{y}}$ in the result, and solving for the control input $\mathbf{u}$

$$\mathbf{u} = \hat{\mathbf{b}}^{-1}(-\hat{\mathbf{f}} + \dot{\mathbf{s}}_r - \mathbf{k}\ \mathrm{sgn}(\mathbf{s})) \quad (73)$$

where $\mathbf{k} = \mathrm{diag}(k_1, k_2, k_3, k_4)$ and $\hat{\ }$ indicates that the matrices in Eq. (67) are evaluated for the nominal values of the system parameters and zero wind disturbance.

Note that the term $\mathrm{sgn}(\mathbf{s})$ is discontinuous at $\mathbf{s} = \mathbf{0}$, which causes chatter of the output trajectory about the surface. To avoid this situation, this term is replaced by a saturation function, which is continuous. The modified control input becomes

$$\mathbf{u} = \hat{\mathbf{b}}^{-1}\left(-\hat{\mathbf{f}} + \dot{\mathbf{s}}_r - \mathbf{k}\ \mathrm{sat}\left(\frac{\mathbf{s}}{\boldsymbol{\Delta}}\right)\right) \quad (74)$$

where

$$\mathbf{k}\ \mathrm{sat}\left(\frac{\mathbf{s}}{\Delta}\right) = \begin{bmatrix} k_1\ \mathrm{sat}(s_1/\delta_1) \\ k_2\ \mathrm{sat}(s_2/\delta_2) \\ k_3\ \mathrm{sat}(s_3/\delta_3) \\ k_4\ \mathrm{sat}(s_4/\delta_4) \end{bmatrix} \quad (75)$$

and δ_1–δ_4 are called the boundary layers of the surfaces.

When there is no uncertainty in the input–output description and no external disturbance, the Lyaponuv function (71) is satisfied by any positive k_i ($i = 1, \ldots, 4$). In the presence of uncertainty and disturbance, k_i's must be large enough such that a new Lyaponuv function is satisfied. The new function is defined as

$$s_i.\dot{s}_i \le -\eta_i|s_i|, \qquad \eta_i > 0, \qquad i = 1, \ldots, 4 \quad (76)$$

where $\eta_i > 0$ determines the convergence speed to the surface. To satisfy Eq. (76), k_i's must be calculated using

https://doi.org/10.1017/S0263574707003670 Published online by Cambridge University Press

the following relation[25]

$$(1-\Delta_{ii})k_i + \sum_{j\neq i}^{4}\Delta_{ij}k_j = F_i + \eta_i + \sum_{j=1}^{4}\Delta_{ij}|-\hat{f}_j + \dot{s}_{rj}|, \quad i=1,..,4 \tag{77}$$

in which the following bounds are assumed for the parameter uncertainties and disturbances in order to determine the controller nonlinearity gains

$$|\mathbf{f}-\hat{\mathbf{f}}| \leq \mathbf{F} \tag{78}$$

$$\mathbf{b} = (\mathbf{I}+\boldsymbol{\delta})\hat{\mathbf{b}}, \qquad |\delta_{ij}| \leq \Delta_{ij}, \qquad i,\ j=1,..,4 \tag{79}$$

When k_i's satisfy Eq. (77), it is guaranteed that the outputs reach the surfaces despite the existence of parameter uncertainties and disturbances defined in Eqs. (78) and (79). After the outputs are on their corresponding surfaces, s_1–s_4 are zero. Therefore, the outputs slide on the surface to their desired values as is observed from Eq. (68).

Note that the control law (74) requires the formation parameters, their first-order derivatives, and the states of the leader(s) and the follower helicopter at any given time. The states of the leader helicopter(s), especially their Euler angles and angular velocities are difficult to measure using vision sensors on the follower helicopter. Therefore, it is assumed that the leader(s) communicate their states with the follower. Once the follower is aware of the states of the leader(s), it can calculate the formation parameters based on the leader(s)' and its own positions, and the rate of formation parameters based on the leader(s)' and its own linear and angular velocities. The required communication bandwith is bounded and is not a function of the number of helicopters in the formation because the controllers are decentralized. Each helicopter has to receive information from at most two helicopters and send information to at most two helicopters.

5. Simulations

Numerical simulations show the effectiveness of the controller design. Three sets of simulations are presented in this section. In these simulations, all the controller parameters, λ_i's ($i=1,\ldots,4$) are selected to be 0.3 for both the l–α and the l–l controllers. For this application, the boundary layers for the length outputs l_{12}, l_{13}, l_{23}, and z_{12} are assumed to be 0.1 m/s, whereas the boundary layer for the angular outputs α_{12}, β_{123}, ψ_2, and ψ_3 are selected to be $\pi/40$ rad/s. These boundary layers minimize the chatter about the surface. The controller nonlinearity gains are set to $k_i = 100$ for both the controllers. The numerical values of the nominal dynamic parameters of the helicopters are corresponding to the Ikarus ECO small electric helicopter, which have been determined by experimental parameter identification[26]

$$\hat{m} = 1.36 \text{ kg}; \qquad \hat{I}_{xx} = 0.137 \text{ kg.m}^2, \qquad \hat{I}_{yy} = 0.221 \text{ kg.m}^2, \qquad \hat{I}_{zz} = 0.0323 \text{ kg.m}^2;$$
$$\hat{l}_{\mathrm{r}} = 0.1 \text{ m}, \qquad \hat{l}_{\mathrm{t}} = 0.635 \text{ m}, \qquad d = 1.0 \text{ m}. \tag{80}$$

Also, in the simulation where the wind disturbance is included, the direction of the wind is assumed to be along the negative y-axis of the inertial frame. The shape of the helicopter fuselage is approximated by a box to estimate the wind forces, where L is the length, and H is the height of the helicopter fuselage. Also, ρ is the air density, and v_{w} is the wind velocity. The following numerical values are used:

$$L = 0.3 \text{ m}, \qquad H = 0.2 \text{ m}, \qquad \rho = 1.2 \text{ kg/m}^3, \qquad v_{\mathrm{w}} = 10 \text{ m/s}. \tag{81}$$

This wind results in an approximate force of $F_{\mathrm{w}} = \frac{1}{2}\rho v_{\mathrm{w}}^2 HL = 3.6$ N, which is 27% of the helicopter's weight (or main rotor's thrust at hovering condition). The maximum rotor's thrust for this helicopter is about 30 N. These data have been used with the dynamic model when the effect of the wind on the helicopter's performance is to be shown. Note that the formation controllers are not aware of the presence of the wind forces and do not directly compensate for them.

5.1. The l–α control scheme

The first simulation set confirms the robustness of the l–α controller. The control law (74) calculates the required inputs $\mathbf{u}$ without being aware of the presence or absence of the wind. These control commands are directly applied to the equations of motion of the follower helicopter. In the no-wind simulation case, the equations of motion as listed in Section 2 are used for integration. In the case where wind is present, a force term representing the wind force is added to the translational equations of motion of the follower.

Figure 6 shows the paths of the motion for the two cases. Two coincident lines show the specified motion of the leader helicopter in no-wind and lateral wind situations. The leader is moving in a straight line with a constant speed of 1 m/s. Note that the steady state roll angle of the lead helicopter is different when the lateral wind is or is not blowing. This fact is reflected in the figure, in which pairs of leader

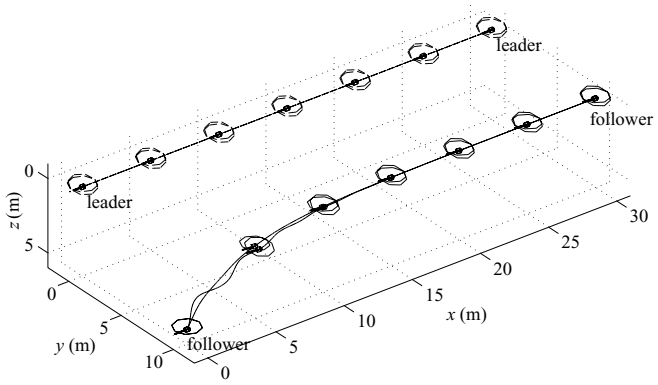

Fig. 6. Path of the motion for the l–α scheme. The follower robustly follows the leader with a given relative position despite a 10 m/s lateral wind. The effect of the wind on the path of the follower is negligible.

https://doi.org/10.1017/S0263574707003670 Published online by Cambridge University Press

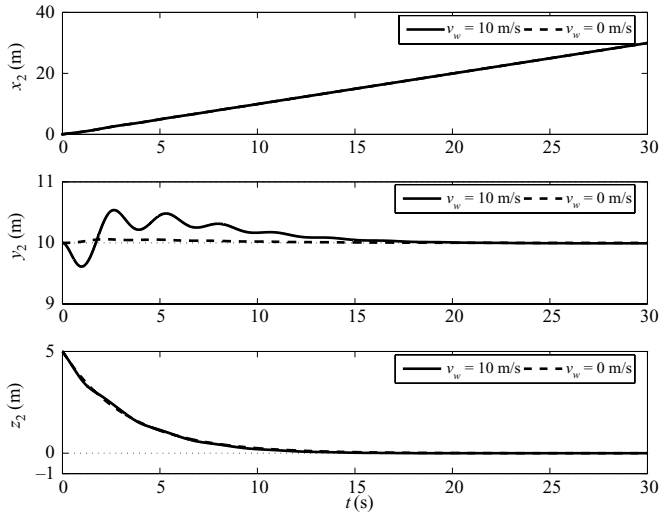

Fig. 7. Position trajectories for the l–α scheme. The follower's position trajectories in the presence and the absence of the wind disturbance are fairly close. The difference in the y component is because the follower tries to reach a steady state roll angle to resist the lateral wind force when the wind is present.

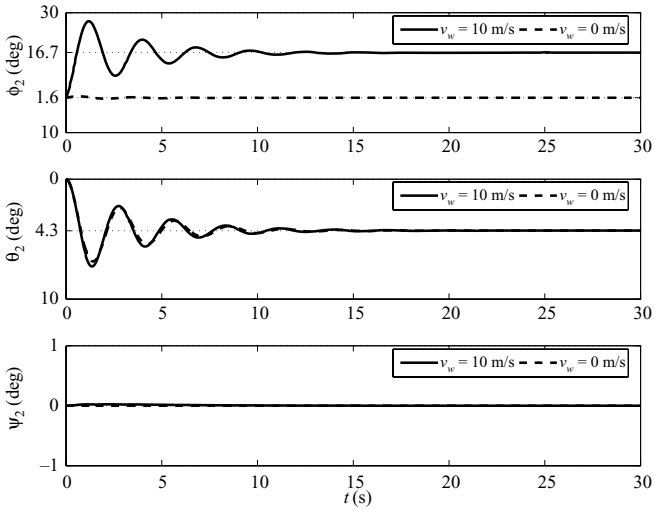

Fig. 8. Orientation trajectories for the l–α scheme. The follower's orientation trajectories in the presence and the absence of the wind disturbance are fairly close, except for the roll angle. The steady state roll angle is larger when wind is present, because the follower tries to counteract the lateral wind force.

helicopter icons are coincident while they have a different roll orientation. The follower is initially at rest at point (0, 10, 5) m with zero orientation angles. At time zero, helicopter 2 receives a command to follow the leader with a lateral distance of $l_{12}^d = 10\,\text{m}$, a view angle of $\alpha_{12}^d = \pi/2$ rad, a vertical distance of $z_{12}^d = 0\,\text{m}$, and a yaw angle of $\psi_2^d = 0\,\text{rad}$. The simulation is run for 30 s. As seen in the figure, there is not much difference in the steady-state path of the follower in the two cases. The transient portion of the paths are somehow different, because the follower has to reach a larger roll-angle equilibrium position when there is wind.

Figure 7 shows the global position components of the follower helicopter. It can be seen that the x and z components of motion are not affected by the presence of the lateral wind. Only the y component is initially disturbed because of the wind. However, the controller is successful in rejecting the disturbances and bringing the y component to the desired equilibrium state.

Figure 8 shows the orientation of the follower helicopter. The pitch and yaw motions are minimally affected by the wind force. The roll angle reaches 1.6° at the steady state when there is no wind. This small angle is necessary such that the lateral components of the main rotor and the tail rotor forces reach an equilibrium, which is necessary for the helicopter to move on a straight line. The steady-state roll angle is larger (16.7°) when a lateral wind is blowing. In such a situation, the helicopter has to lean against the wind direction to equalize the wind force with the lateral component of the main rotor thrust.

Figure 9 shows the four l–α formation parameters or the control outputs. Once again, it is seen that the effect of the wind on these outputs is minimal. The steady-state values of the formation parameters do not experience any offsets. The values approach the desired values despite the wind disturbance. The control points of the leader and the follower helicopters keep a distance of 10 m ($l_{12} = 10$ m). The helicopters move side by side ($\alpha_{12} = 90°$) and at the same height ($z_{12} = 0$ m). And the follower helicopter faces straight ahead ($\psi_2 = 0°$).

Figure 10 shows the four helicopter control inputs. The thrust force T is higher when the wind blows, because it has to provide a lateral component to counterbalance the lateral wind force. The larger roll angle in the wind situation allows for this component. Since the main rotor axis does not pass through the helicopter's center of mass, the main rotor's thrust generates a moment about this point. This moment is counterbalanced by the pitch moment. An increased thrust requires a higher pitch moment. This fact is reflected in the M_θ plot. The tail-rotor thrust also has to equalize the reaction torque on the fuselage caused by T. Hence, a higher tail-rotor thrust T_T is required when the wind is present.

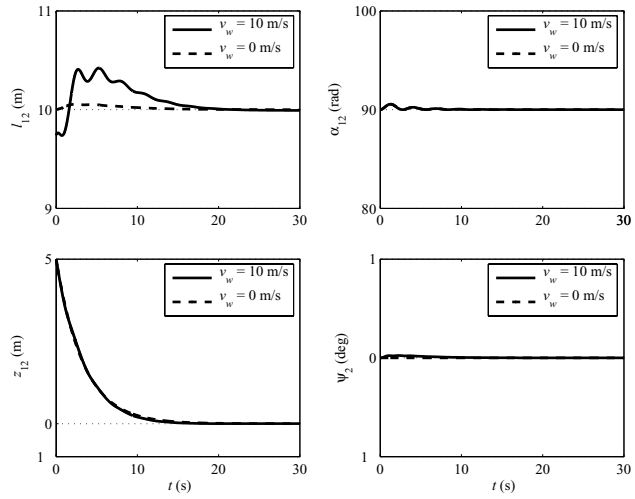

Fig. 9. Output trajectories for the l–α scheme. The formation parameters' steady-state values are not significantly affected by the lateral wind. The initial disturbance in l_{12} is because the follower tries to reach an equilibrium roll angle to counteract the lateral wind force.

https://doi.org/10.1017/S0263574707003670 Published online by Cambridge University Press

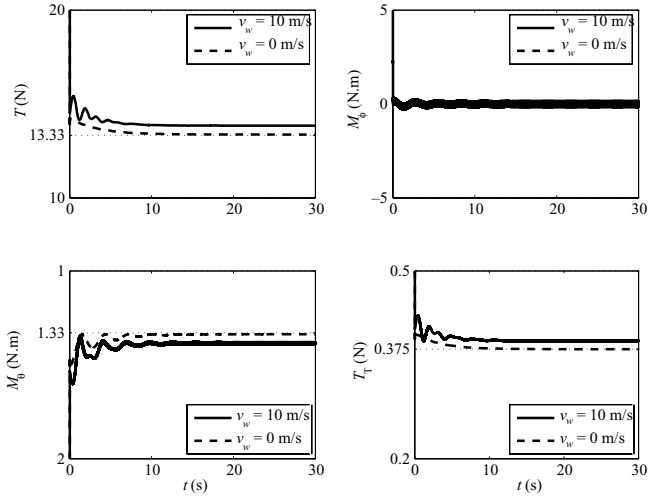

Fig. 10. Input history for the l–α scheme. The required thrust T when wind exists is higher than that of the no-wind situation. Other control inputs are also higher in the presence of wind to counterbalance the higher thrust force, except M_ϕ. This is because T does not produce a moment about the helicopter's roll axis.

5.2. The l–l control scheme

In this section, the robustness of the l–l controller is shown by simulations. It is assumed that two leaders are flying on parallel straight lines and a follower is assigned to follow them. This scenario is simulated for two different cases, one with and one without a lateral wind. The presence or absence of the wind is not known to the controller. However, a force term representing the wind force is added to the translational equations of motion of the follower during the numerical integration.

The paths of the motion of the leaders and the follower are shown in Fig. 11 for the two cases. A straight line motion with a speed of 1 m/s is defined for the leaders. The follower is initially at rest at point $(-5, 0, 5)$ m with zero orientation angles. At time zero, helicopter 3 receives a command to follow the leaders with equal distance of $l_{13}^d = l_{23}^d = 5$ m, while the desired formation plane is horizontal ($\beta_{123}^d = \pi/2$ rad). The desired yaw angle of the follower is $\psi_3^d = 0$ rad. The simulation is run for 30 s. The figure shows

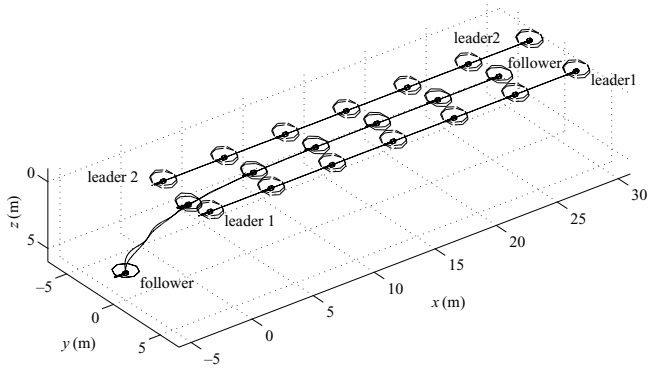

Fig. 11. Path of the motion for the l–l scheme. The effect of the wind on the path of the follower is negligible. Despite a 10 m/s lateral wind, the follower robustly follows the leaders with a given relative position.

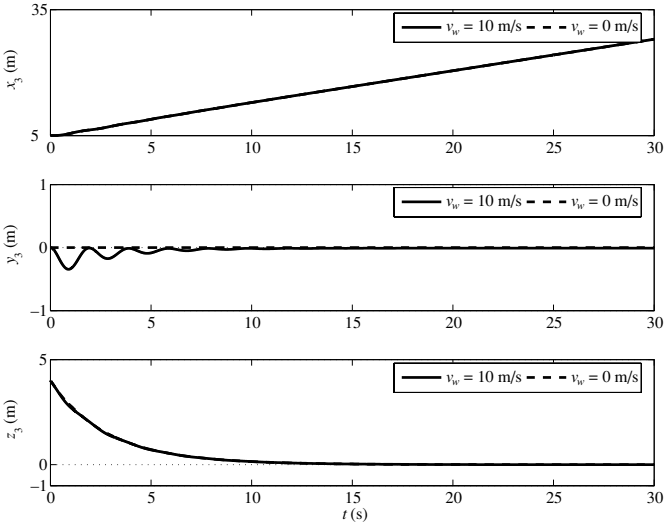

Fig. 12. Position trajectories for the l–l scheme. The follower's position trajectories for the zero and nonzero wind force situations are very similar. The difference in the y component is because the follower tries to reach a larger steady-state roll angle at which it can resist the lateral wind force when the wind is present.

a minimal difference in the steady-state path of the follower in the two cases.

The global position components of the follower helicopter are plotted in Fig. 12. The lateral wind does not affect x and z components of motion, whereas the y component is initially disturbed. However, the controller successfully brings the y component to the desired equilibrium state.

The orientation of the follower helicopter can be seen in Fig. 13. Once again, the steady-state equilibrium of the roll angles are 1.6 and 16.7° for the with and without wind cases, respectively. These values are equal to the result of the l–α controller, because the equilibrium roll angle is inherent in the dynamics of the helicopter.

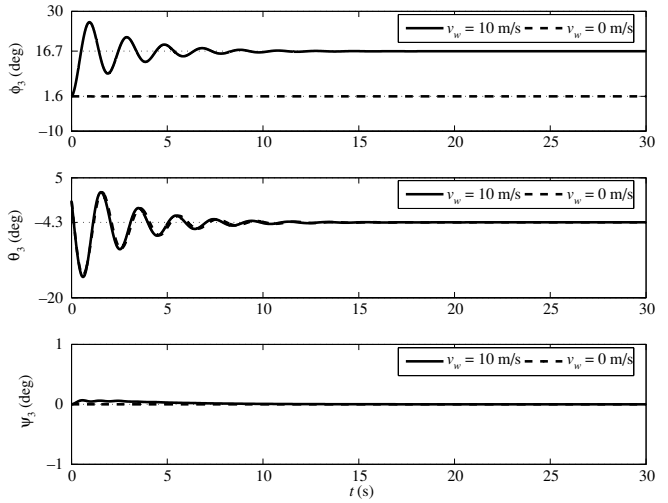

Fig. 13. Orientation trajectories for the l–l scheme. Except for the roll angle, the follower's orientation trajectories in the presence and the absence of the wind disturbance are fairly close. Since the follower tries to counteract the lateral wind force, the steady-state roll angle is larger when wind is present.

https://doi.org/10.1017/S0263574707003670 Published online by Cambridge University Press

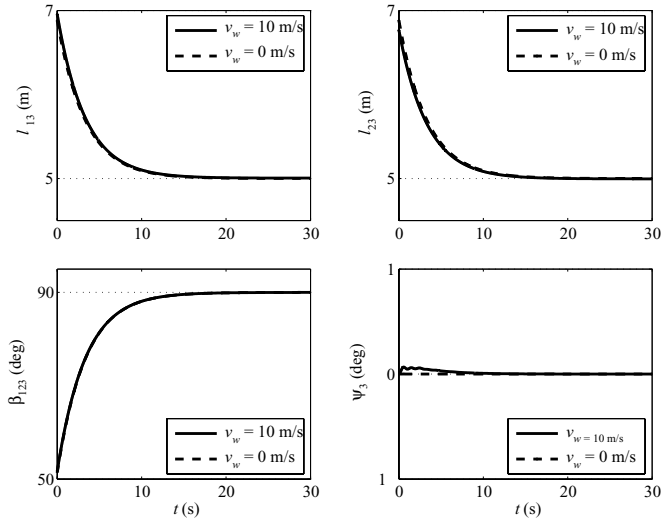

Fig. 14. Output trajectories for the l–l scheme. The formation parameters' steady-state values are not significantly affected by the lateral wind. The difference between the output trajectories for the two wind conditions is negligible.

The four l–l formation parameters or the control outputs are, presented in Fig. 14. The steady-state values of the formation parameters do not experience any offsets in any case. The control points of the follower stay at a distance of 5 m with the control points of both the leaders during the motion ($l_{13} = l_{23} = 5$ m). The follower helicopter moves at the same height of the two leaders ($\beta_{123} = 90°$). And the follower helicopter faces straight ahead as instructed ($\psi_3 = 0°$).

The four helicopter control inputs are shown in Fig. 15. The control forces are, in general, similar to that of the l–α controller. However, the inputs show more chatter. The chatter can be reduced by fine tuning the controller-gain nonlinearity and the boundary layer for the l–l controller.

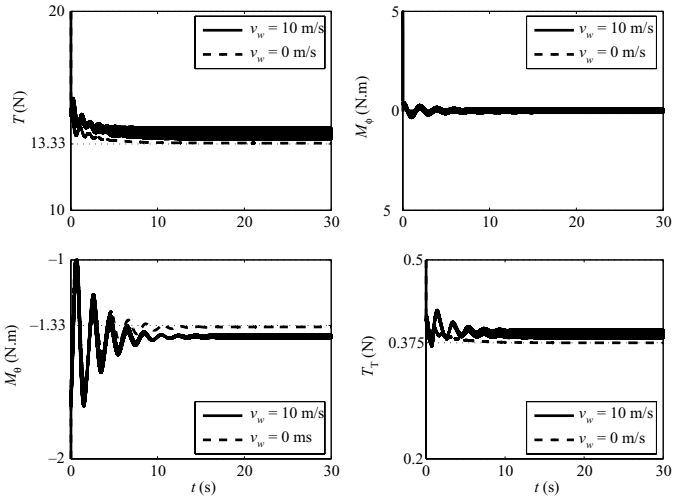

Fig. 15. Input history for the l–l scheme. The required thrust T when wind exists is higher than that of the no-wind situation. Other control inputs are also higher in the presence of wind to counterbalance the higher thrust force, except M_ϕ. This is because T does not produce a moment about the helicopter's roll axis.

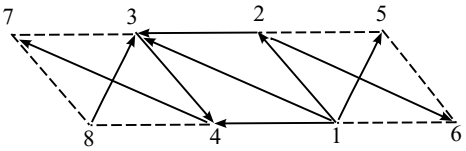

Fig. 16. Eight helicopters in a planar rectangular formation. Helicopter 1 is the group leader. Helicopter 2 follows 1 using the l–α scheme. Helicopter 3 follows 2 and 1 using the l–l scheme. Helicopter 4 follows 3 and 1 using the l–l scheme. Helicopters 5, 6, 7, and 8 follow 1, 2, 4, and 3, respectively, using the l–α scheme.

5.3. General three-dimensional formation

The developed formation control schemes can be used as building blocks to define any three-dimensional formation for groups of autonomous helicopters. By changing the desired formation parameters, the user can change the formation structure of the group. This concept is shown by simulation.

In this section, the formation flight of eight helicopters is simulated as an example to show the configurability of a formation structure built using the developed l–α and l–l schemes. Eight helicopters are interconnected as shown in Fig. 16. They initially make a rectangular formation with a grid size of 5 m while moving forward with a constant speed of 1 m/s. At time zero, they are commanded to form a spatial cubic formation with a 5 m dimension as presented in Fig. 17. This is equivalent to defining a new set of formation parameters for helicopters 5–8.

The described change of formation is simulated for two different cases to show the robustness of the controllers in the presence of parameter uncertainty. In both the cases, the control law is calculated based on the helicopters' nominal parameters listed in Eq. (80). However, the inertia parameters used with the dynamic model to simulate the response of the helicopters are different for the two cases. In the first case, the nominal mass and moment of inertia are used. In the second case, the helicopters' mass and moment of inertia are assumed to be 20% higher than the nominal values.

Figure 18 shows the 35 s motion of the helicopters for the two cases. The curves that show the path of the motion of each helicopter for the two different cases are either very close or completely coincident with each other. This shows the robustness of the formation controllers to parameter uncertainty. Furthermore, while the helicopters start their change of formation, a lateral wind starts to blow. The wind

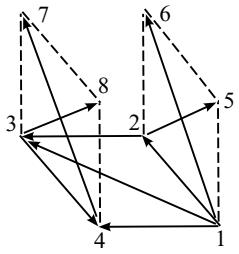

Fig. 17. Eight helicopters in a spatial cubic formation. The formation structure of these eight helicopters is the same as that of the group shown in Fig. 16. However, the desired formation parameters for the helicopters 5–8 are different than that of the planar configuration of Fig. 16.

https://doi.org/10.1017/S0263574707003670 Published online by Cambridge University Press

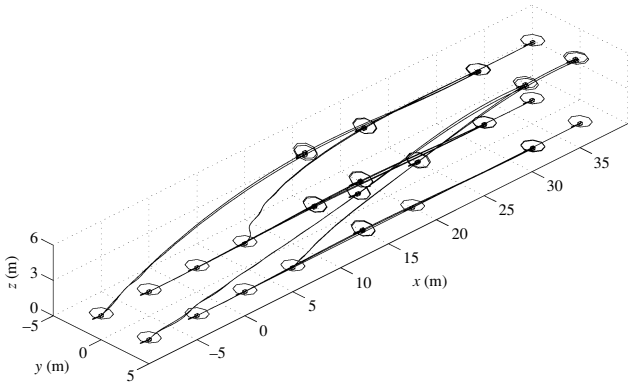

Fig. 18. Formation change of a group of eight helicopters with and without model-inertia uncertainty. The helicopters are initially in a planar rectangular formation as defined in Fig. 16. They change formation while continuing their maneuver after a new set of desired formation parameters are defined. The curves showing the path of the helicopters for the cases of 0% and +20% inertia uncertainty are either very close or coincident.

reaches its peak speed of 10 m/s at 17.5 s, and vanishes gradually after that, until it totally vanishes at 35 s. The roll angle of the helicopters (shown at middle of the path at 17.5 s) reflects the effect of the wind. The helicopters successfully achieve the new desired formation after 35 s despite the wind and inertia uncertainties.

6. Conclusions

The formation control problem for small autonomous helicopters was considered. Two decentralized three-dimensional formation control schemes were introduced for a general formation control. The controller design was based on a six-degree-of-freedom dynamic model with forces and moments as the actuation means. Sliding-mode control method was used due to its robustness in the presence of disturbances. The effectiveness of the controllers was shown via simulations. It was shown that by using the two formation-control schemes, any spatial formation can be defined for a number of helicopters. The helicopters are able to achieve the defined formations even in the presence of rather high environmental disturbances and up to 20% uncertainty in the mass and moment of inertia.

References

1. T. Sugar and V. Kumar, "Decentralized Control of Cooperating Mobile Manipulators," in *Proceedings of the IEEE International Conference on Robotics and Automation*, Leuven, Belgium (May 1998) pp. 2916–2921.
2. J. P. Desai, "A graph theoretic approach for modeling mobile robot team formations," *J. Robot. Syst.* **19**(11), 511–525 (2002).
3. H. Yamaguchi, "Cooperative hunting behavior by mobile-robot troops," *Int. J. Robot. Res.* **18**(9), 931–940 (1999).
4. S. Sheikholeslam and C. A. Desoer, "Control of interconnected nonlinear dynamical systems: The platoon problem," *IEEE Trans. Autom. Control* **37**, 806–810 Jun. (1992).
5. P. K. C. Wang and F. Y. Hadaegh, "Coordination and control of multiple microspacecraft moving in formation," *J. Astronaut. Sci.* **44**(3), 315–355 (1996).
6. P. K. C. Wang, F. Hadaegh and K. Lau, "Synchronized formation rotation and attitude control of multiple free-flying spacecraft," *AIAA J. Guid. Control Dyn.* **22**, 28–35, Jan. (1999).
7. F. Y. Hadaegh, W. M. Lu and P. K. C. Wang, "Adaptive Control of Formation Flying Spacecraft for Interferometry," Large Scale Systems: Theory and applications 1998. Proceedings volume from the 8th IFAC/IFORS/IMAC/IFIP Symposium, 1999, pt. 1, pp. 117–122 vol. 1.
8. V. Kapila, A. G. Sparks, J. M. Buffington and Q. Yan, "Spacecraft formation flying: Dynamics and control," *J. Guid. Control Dyn.* **23**, 561–564, May–Jun. (2000).
9. W. M. Spears, D. F. Spears and R. Heil, "A formal analysis of potential energy in a multi-agent system," *Lect. Notes Artif. Intell. (Subser. Lect. Notes Comput. Sci.)* **3228**, 131–145 (2004).
10. T. Balch and R. C. Arkin, "Behavior-based formation control for multirobot teams," *IEEE Trans. Robot. Autom.* **14**, 926–939, Dec. (1998).
11. X. Yun, G. Alptekin and O. Albayrak, "Line and circle formation of distributed physical mobile robots," *J. Robot. Syst.* **14**(2), 63–76 (1997).
12. O. Khatib, "Real-time obstacle avoidance for manipulators and mobile robots," *Int. J. Robot. Res.* **5**(1), 90–99 (1986).
13. C. R. McInnes, "Autonomous ring formation for a planar constellation of satellites," *J. Guid. Control Dyn.* **18**(5), 1215–1217 (1995).
14. M. R. Anderson and A. C. Robbins, "Formation Flight as a Cooperative Game," *Proceedings of the AIAA Guidance, Navigation, and Control Conferences*, AIAA-984124, Boston, MA (1998) pp. 244–251.
15. P. McDowell, J. Chen and B. Bourgeois, "UUV Teams, Control From a Biological Perspective," *Proceedings of the IEEE Oceans Conference Record*, Mississippi (2002) **1**, pp. 331–337.
16. W. Ren and R. W. Beard, "Decentralized scheme for spacecraft formation flying via the virtual structure approach," *J. Guid. Control Dyn.* **27**(1), 73–82 (2004).
17. M. A. Lewis and K.-H. Tan, "High precision formation control of mobile robots using virtual structures," *Auton. Robots* **4**, 387–403 (1997).
18. R. W. Beard and F. Y. Hadaegh, "Constellation Templates: An Approach to Autonomous Formation Flying," *Proceedings of the World Automation Congress*, Anchorage, AK, (May 1998) pp. 177.1–177.6.
19. I. F. Ihue, R. Skjetne and T. I. Fossen, "Nonlinear Formation Control of Marine Craft With Experimental Results," *Proceedings of the IEEE Conference on Decision and Control* (2004) Nassau, Bahamas **1**, pp. 680–685.
20. J. M. Eklund, J. Sprinkle and S. Sastry, "Implementing and Testing a Nonlinear Model Predictive Tracking Controller for Aerial Pursuit/Evasion Games on a Fixed Wing Aircraft," *Proceedings of the American Control Conference*, Portland, OR (2005) **3**, pp. 1509–1514.
21. R. Vidal, S. Rashid, C. Sharp, O. Shakernia, J. Kim and S. Sastry, "Pursuit-Evasion Games With Unmanned Ground and Aerial Vehicles," *Proceedings of the IEEE International Conference on Robotics and Automation*, Seoul, Korea (2001) **3**, pp. 2948–2955.
22. S. Zelinski, T. J. Koo and S. Sastry, "Optimization-Based Formation Reconfiguration Planning for Autonomous Vehicles," *Proceedings of the IEEE International Conference on Robotics and Automation*, Taipei, Taiwan (2003) **3**, pp. 3758–3763.
23. H. Chung and S. S. Sastry, "Autonomous Helicopter Formation Using Model Predictive Control," *Proceedings of the Collection of Technical Papers—AIAA Guidance, Navigation, and Control Conference* (2006) **1**, pp. 459–473.
24. J. H. Ginsberg, *Advanced Engineering Dynamics*, 2nd ed. (Cambridge University Press, Cambridge, UK, 1998).
25. J. E. Slotine and W. Li, *Applied Nonlinear Control* (Prentice-Hall, Englewood Cliffs, NJ 1991).
26. S. K. Kim and D. M. Tilbury, "Mathematical modeling and experimental identification of an unmanned helicopter robot with flybar dynamics," *J. Robot. Syst.* **21**(3), 95–116 (2004).

https://doi.org/10.1017/S0263574707003670 Published online by Cambridge University Press

Appendix: Details of the Kinematic Analysis for the *l–l* Control Scheme

A.1. Velocity

The rate of change of the direction parameter of the *l–l* formation plane, β_{123}, as defined in Fig. 5, can be calculated via two different approaches. In one approach, as shown in the body of the paper [Section 3.2.1, Eqs. (43) and (44)], the relative velocity control of points p_1 and p_3 can be used. The second approach can be formulated based on the relative velocity of the control points p_2 and p_3. Both approaches lead to the same result for $\dot{\beta}_{123}$, although the two mathematical descriptions of $\dot{\beta}_{123}$ look different. Here, it is shown that the two descriptions are equivalent.

If the second approach is taken, an equation similar to Eq. (43) can be written

$$\mathbf{v}_{p3}^{(f)} = \mathbf{v}_{p2}^{(f)} + \boldsymbol{\omega}_f^{(f)} \times \mathbf{l}_{23}^{(f)} + \dot{\mathbf{l}}_{23}^{(f)}. \tag{A1}$$

$\dot{\beta}_{123}$ can be found by simplifying the third component of Eq. (A1)

$$\dot{\beta}_{123} = \frac{v_{p3z}^{(f)} - v_{p2z}^{(f)} + \omega_{f2} l_{23} \cos\gamma_{23}}{l_{23}\sin\gamma_{23}}. \tag{A2}$$

The third component of Eq. (42) indicated that

$$v_{p2z}^{(f)} = v_{p1z}^{(f)} - \omega_{f2} l_{12}. \tag{A3}$$

Substituting Eq. (A3) into (A2) results in

$$\dot{\beta}_{123} = \frac{v_{p3z}^{(f)} - v_{p1z}^{(f)} + \omega_{f2}(l_{12} + l_{23}\cos\gamma_{23})}{l_{23}\sin\gamma_{23}}. \tag{A4}$$

According to Fig. 4, one can write $\mathbf{l}_{12}^{(f)} + \mathbf{l}_{23}^{(f)} = \mathbf{l}_{13}^{(f)}$. In component notation, this can be expressed as

$$l_{12} + l_{23}\cos\gamma_{23} = l_{13}\cos\gamma_{13} \tag{A5}$$

$$l_{23}\sin\gamma_{23} = l_{13}\sin\gamma_{13}. \tag{A6}$$

Substituting Eqs. (A5) and (A6) into (A4) results in

$$\dot{\beta}_{123} = \frac{v_{p3z}^{(f)} - v_{p1z}^{(f)} + \omega_{f2} l_{13}\cos\gamma_{13}}{l_{13}\sin\gamma_{13}} \tag{A7}$$

which is identical to Eq. (44).

A.2. Acceleration

The second derivative of the direction parameter of the *l–l* formation plane, β_{123} appeared in two different equations, as shown in the body of the paper [Section 3.2.1, Eqs. (52) and (54)]. Although the two mathematical descriptions in Eqs. (52) and (54) for $\ddot{\beta}_{123}$ look different, they are actually equivalent. Here, it is shown that the two descriptions are equivalent.

Equation (51) is repeated here for reference.

$$\begin{bmatrix} \ddot{l}_{13}\cos\gamma_{13} - \alpha_{f3} l_{13}\sin\gamma_{13} \\ \ddot{l}_{13}\sin\gamma_{13} + \alpha_{f3} l_{13}\cos\gamma_{13} \\ \ddot{\beta}_{123} l_{13}\sin\gamma_{13} \end{bmatrix} = \mathbf{a}_{c3}^{(f)} + \boldsymbol{\omega}_3^{(f)} \times \mathbf{d}^{(f)} + \mathbf{N}_1 - \mathbf{M}_1. \tag{A8}$$

Equation (54) can be rearranged in the form of Eq. (51) as

$$\begin{bmatrix} \ddot{l}_{23}\cos\gamma_{23} - \alpha_{f3} l_{23}\sin\gamma_{23} \\ \ddot{l}_{23}\sin\gamma_{23} + \alpha_{f3} l_{23}\cos\gamma_{23} \\ \ddot{\beta}_{123} l_{23}\sin\gamma_{23} \end{bmatrix} = \mathbf{a}_{c3}^{(f)} + \boldsymbol{\omega}_3^{(f)} \times \mathbf{d}^{(f)} + \mathbf{N}_2 - \mathbf{M}_2. \tag{A9}$$

Since $l_{23}\sin\gamma_{23} = l_{13}\sin\gamma_{13}$ (A6), the coefficient of $\ddot{\beta}_{123}$ on the right-hand side of Eqs. (A8) and (A9) are equal. If it can be shown that the third components of the left-hand side of these equations are also equal, it can be concluded that they result in the same $\ddot{\beta}_{123}$. The difference of the third component of the left-hand sides of Eqs. (A8) and (A9) is [see Eqs. (49), (50), (56), and (57)]

$$\begin{aligned}(\mathbf{N}_1 - \mathbf{N}_2)_z - (\mathbf{M}_1 - \mathbf{M}_2)_z = \big[&\big(\mathbf{a}_{p2}^{(f)} - \mathbf{a}_{p1}^{(f)}\big) - \boldsymbol{\omega}_f^{(f)} \\ &\times \big(\boldsymbol{\omega}_f^{(f)} \times \big(\mathbf{l}_{13}^{(f)} - \mathbf{l}_{23}^{(f)}\big)\big) - 2\boldsymbol{\omega}_f^{(f)} \times \big(\dot{\mathbf{l}}_{13}^{(f)} - \dot{\mathbf{l}}_{23}^{(f)}\big)\big]_z \\ &- [-\alpha_{f2}(l_{13}\cos\gamma_{13} - l_{23}\cos\gamma_{23})].\end{aligned} \tag{A10}$$

Since $\mathbf{l}_{13}^{(f)} - \mathbf{l}_{23}^{(f)} = \mathbf{l}_{12}^{(f)}$ (Fig. 4) and according to Eq. (A5), the previous equation can be simplified as

$$\begin{aligned}(\mathbf{N}_1 - \mathbf{N}_2)_z - (\mathbf{M}_1 - \mathbf{M}_2)_z = \big[&\big(\mathbf{a}_{p2}^{(f)} - \mathbf{a}_{p1}^{(f)}\big) - \boldsymbol{\omega}_f^{(f)} \\ &\times \big(\boldsymbol{\omega}_f^{(f)} \times \mathbf{l}_{12}^{(f)}\big) - 2\boldsymbol{\omega}_f^{(f)} \times \dot{\mathbf{l}}_{12}^{(f)}\big]_z - [-\alpha_{f2} l_{12}].\end{aligned} \tag{A11}$$

The right-hand side of the previous equation is zero according to Eq. (46)

$$(\mathbf{N}_1 - \mathbf{N}_2)_z - (\mathbf{M}_1 - \mathbf{M}_2)_z = 0. \tag{A12}$$

This means that the third components of the right-hand side of Eqs. (A8) and (A9) are equal and they result in the same values for $\ddot{\beta}_{123}$.

https://doi.org/10.1017/S0263574707003670 Published online by Cambridge University Press